Dendritic cell targeting virus-like particle delivers mRNA for in vivo immunization

Di Yin
Key Laboratory of Systems Biomedicine (Ministry of Education), Shanghai Center for Systems Biomedicine, Shanghai Jiao Tong University

Sikai Ling
Key Laboratory of Systems Biomedicine (Ministry of Education), Shanghai Center for Systems Biomedicine, Shanghai Jiao Tong University

Xiaolong Tian
MOE/NHC/CAMS Key Laboratory of Medical Molecular Virology, School of Basic Medical Sciences, Shanghai Medical College, Fudan University, Shanghai, China

Yang Li
Key Laboratory of Systems Biomedicine (Ministry of Education), Shanghai Center for Systems Biomedicine, Shanghai Jiao Tong University

Zhijue Xu
Key Laboratory of Systems Biomedicine (Ministry of Education), Shanghai Center for Systems Biomedicine, Shanghai Jiao Tong University

Hewei Jiang
Key Laboratory of Systems Biomedicine (Ministry of Education), Shanghai Center for Systems Biomedicine, Shanghai Jiao Tong University

Xue Zhang
Key Laboratory of Systems Biomedicine (Ministry of Education), Shanghai Center for Systems Biomedicine, Shanghai Jiao Tong University

Xiaoyuan Wang
BDgene Therapeutics

Yi Shi
Shanghai Jiao Tong University https://orcid.org/0000-0002-5279-3239

Quanjun Wang
National Beijing Center for Drug Safety Evaluation and Research, State Key Laboratory of Medical Countermeasures and Toxicology, Institute of Pharmacology and Toxicology, Academy of Military Science

Jianjiang Xu
Department of Ophthalmology and Vision Science, Shanghai Eye, Ear, Nose and Throat Hospital, Fudan University

Wei Hong

CAS Key Laboratory of Special Pathogens and Biosafety, Center for Biosafety Mega-Science, Wuhan Institute of Virology, Chinese Academy of Sciences

Heng Xue

CAS Key Laboratory of Special Pathogens and Biosafety, Center for Biosafety Mega-Science, Wuhan Institute of Virology, Chinese Academy of Sciences

hang yang

Wuhan Institute of Virology, Chinese Academy of Sciences https://orcid.org/0000-0001-6750-1465

Yan Zhang

Key Laboratory of Systems Biomedicine (Ministry of Education), Shanghai Center for Systems Biomedicine, Shanghai Jiao Tong University

Lintai Da

Key Laboratory of Systems Biomedicine (Ministry of Education), Shanghai Center for Systems Biomedicine, Shanghai Jiao Tong University

Ze-Guang Han

Shanghai Jiao Tong University

Sheng-ce Tao

Shanghai Jiao Tong University https://orcid.org/0000-0002-9210-1823

Jiaxu Hong

Key Laboratory of Myopia of State Health Ministry and Key Laboratory of Visual Impairment and Restoration of Shanghai, Eye, Ear, Nose and Throat Hospital, Fudan University https://orcid.org/0000-0001-9912-633X

Tianlei Ying

Fudan University https://orcid.org/0000-0002-9597-2843

Yujia Cai (**yujia.cai@sjtu.edu.cn**)

Key Laboratory of Systems Biomedicine (Ministry of Education), Shanghai Center for Systems Biomedicine, Shanghai Jiao Tong University, Shanghai https://orcid.org/0000-0002-2955-7289

Article

Keywords: SARS-CoV-2, HSV-1, Vaccine, mRNA, Dendritic cell

Posted Date: December 1st, 2021

DOI: https://doi.org/10.21203/rs.3.rs-1096471/v1

Dendritic cell targeting virus-like particle delivers mRNA for in vivo immunization

Di Yin[1,#], Sikai Ling[1,#], Xiaolong Tian[2], Yang Li[1], Zhijue Xu[1], Hewei Jiang[1], Xue Zhang[1], Xiaoyuan Wang[3], Yi Shi[4], Quanjun Wang[5], Jianjiang Xu[6], Wei Hong[7,8], Heng Xue[7,8], Hang Yang[7,8], Yan Zhang[1], Lintai Da[1], Ze-guang Han[1], Sheng-ce Tao[1], Tianlei Ying[2], Jiaxu Hong[6,*], and Yujia Cai[1,*]

[1]*Key Laboratory of Systems Biomedicine (Ministry of Education), Shanghai Center for Systems Biomedicine, Shanghai Jiao Tong University, Shanghai 200240, China.*

[2]*MOE/NHC/CAMS Key Laboratory of Medical Molecular Virology, School of Basic Medical Sciences, Fudan University, Shanghai 200032, China.*

[3]*BDgene Therapeutics, Shanghai 200240, China.*

[4]*Bio-X Institutes, Key Laboratory for the Genetics of Developmental and Neuropsychiatric Disorders, Shanghai Jiao Tong University, Shanghai 200030, China.*

[5]*National Beijing Center for Drug Safety Evaluation and Research, State Key Laboratory of Medical Countermeasures and Toxicology, Institute of Pharmacology and Toxicology, Academy of Military Sciences, Beijing 100850, China.*

[6]*Department of Ophthalmology and Vision Science, Shanghai Eye, Ear, Nose and Throat Hospital, Fudan University, Shanghai 200031, China.*

[7]*CAS Key Laboratory of Special Pathogens and Biosafety, Center for Biosafety Mega-Science, Wuhan Institute of Virology, Chinese Academy of Sciences, Wuhan 430071, China.*

[8]*University of Chinese Academy of Sciences, Beijing 100049, China.*

[#]These authors contributed equally.

[*]**For correspondence:**

JH: Phone: 86-021-64377134, jiaxu.hong@fdeent.org

YC: Phone: 86-021-34208571, yujia.cai@sjtu.edu.cn

Running title: DC-specific VLP mRNA vaccine

Keywords: SARS-CoV-2; HSV-1; Vaccine; mRNA; Dendritic cell

ABSTRACT

mRNA vaccine was approved clinically in 2020. Future development includes delivering mRNA to dendritic cells (DCs) specifically to improve effectiveness and avoid off-target cytotoxicity. Here, we developed virus-like particles (VLPs) as a DC tropic mRNA vaccine vector and showed the prophylactic effects in both SARS-CoV-2 and HSV-1 infection models. The VLP mRNA vaccine elicited strong cytotoxic T cell immunity and durable antibody response with the spike-specific antibodies that lasted for more than 9 months. Importantly, we were able to target mRNA to DCs by pseudotyping VLP with engineered Sindbis virus glycoprotein and found the DC-targeting mRNA vaccine significantly enhanced the titer of antigen-specific IgG, protecting the hACE-2 mice from SARS-CoV-2 infection. Additionally, we showed DC-targeted mRNA vaccine also protected mice from HSV-1 infection when co-delivering the gB and gD mRNA. Thus, the VLP may serve as an in situ DC vaccine and accelerate the further development of mRNA vaccines.

Vaccines are among the most effective medical interventions in history, reducing the disease burden worldwide significantly. It saves 2.5 million lives worldwide each year by estimation[1]. However, many diseases are still without effective vaccines, including no prophylactic and therapeutic vaccines for infectious viruses including HIV, HSV-1, and HSV-2, etc[2-5]. For some viruses, the existed vaccines are only preventive and do not eliminate the already established infection such as HBV and HPV[6,7]. In terms of non-infectious diseases, the cancer vaccine development is still in early stages with marginal success in clinical trials in treating melanoma and glioblastoma[8,9]. These health threats motivate further development and improvement of vaccine technologies.

The future of mRNA vaccine has been widely recognized since the breakout of severe acute respiratory syndrome coronavirus 2 (SARS-CoV-2) in December 2019 which has dramatically speeded up the development of mRNA vaccines[10]. Two coronavirus disease 2019 (COVID-19) mRNA vaccines, Moderna (mRNA-1273) and Pfizer/BioNTech (BNT162b2), achieved approximately 90-95% efficacy with minimal side effects[11-14]. While SARS-CoV-2 mRNA vaccines have been widely dosed in developed countries and are effective in preventing severe COVID-19 outcomes, the virus transmission is still not under full control[15]. Additionally, the potential of mRNA vaccine beyond the SARS-CoV-2 infection awaits further exploration.

As mRNA are vulnerable to RNA nuclease and cannot enter cells by themselves, a variety of carriers have been developed for mRNA transfer including lipid-nanoparticles (LNPs), polymers, peptides, virus-like replicon particles (VRPs) and dendritic cells (DCs)[16]. LNP is now the first runner due to the success in SARS-CoV-2 vaccines. The current LNP mRNA is unable to control cell specificity and can be taken up by almost any cell type, near or far from the site of injection[17]. DCs are the major antigen-presenting cells (APCs) and critical for vaccine function by 1) instigating the T cell immune responses through antigen processing to T cells[18,19], 2) processing antigens to B-cells and inducing antibody responses[20,21].

The DC-based vaccine has been approved by US FDA in use for the treatment of prostate cancer, however, it was made ex vivo and labour intensive, weakening the availability to a broader population. The DC-targeting strategy makes DC vaccine in situ, therefore, lowering the cost and simplifying the manufacture. Moreover, it has been suspected that non-professional APCs with antigen mRNA in translation may become a target of CD8+ T cell-mediated killing, which has been linked to 'Covid-arm' that develops in some patients after receiving the COVID-19 mRNA vaccine[22,23]. Furthermore, antibody-dependent cellular cytotoxicity (ADCC) may also destroy the cells with antigen proteins inserted into, or secreted and associated with the plasma membrane[22,24]. Targeting DC in situ has been achieved by using pseudotyped lentiviral vectors (LVs) with Sindbis virus glycoprotein as a ligand for DC-SIGN, however, due to the reverse transcription step, the DC-targeting LV vaccine has potential risks of insertional mutagenesis[25]. LNPs have also been conjugated to specific antibodies or ligands to target DC for in vitro and in vivo evaluation, although the evidences for effective LNP based DC-targeting mRNA vaccine are rare[22].

Driven by the need for mRNA delivery vectors with DC specificity to improve antivirus responses while limiting the possible off-target cytotoxicity, here, we developed a virus-like particle (VLP)-based mRNA vaccine technology and showed VLP delivered antigen mRNA elicited strong and durable adaptive immune responses. The specific IgG was maintained at a high level for at least 9 months. Additionally, the VLP-mRNA was also compatible with the intranasal administration route and induced significant mucosal immunity. We found the DC-targeting VLP elicited significantly higher antigen-specific IgG response than the non-specific counterpart. Importantly, the DC-targeting VLP-mRNA vaccine efficiently protected mice from live virus infection in both SARS-CoV-2 and HSV-1 infection models. Together, the VLP is able to deliver mRNA specifically to DCs and may accelerate the further development of mRNA vaccines including against infectious diseases without vaccines and cancers.

Results

Design and characterization of VLP-based SARS-CoV-2 mRNA vaccine. To show the potential of VLP as an mRNA vaccine carrier, we performed a proof-of-concept study by designing a candidate SARS-CoV-2 mRNA vaccine which encodes the full-length spike mRNA composed of a signal peptide from the human heavy chain of IgE and the codon-optimized sequence (Fig. 1a). To increase the stability and expression of the spike, we also introduced two proline substation mutations (K986P/V987P) in the S2 (Fig. 1a)[26]. We have previously shown delivery of Cas9 mRNA with lentivirus-derived VLP mediated efficient genome editing in vivo in the different disease models[27,28], however, it is unclear if VLP can serve as a vaccine platform. To package the full-length spike mRNA into VLPs, we inserted MS2 stem-loop repeats in its 3' terminus between the stop codon and the polyA signal. This design allows the spike mRNA to be internalized via its interaction with the MS2 coat protein fused in the N-terminus of GagPol which can self-assemble into VLP (Fig. 1b). As VSV-G coated lentiviruses are efficiently taken up by APCs and show the high immunogenicity of antigens[29], we therefore firstly pseudotyping VLP with VSV-G by providing the pMD.2G plasmid in the production process. To analyse the morphology of the VLP, we conducted electron microscopy which was in round shape with a size of approximately 100 nm (Fig. 1c).

To find out if spike mRNA has been indeed packaged into lentiviral particles, we performed RT-qPCR on VLP and normalized it to the traditional lentiviral vector which had two copies of RNA. We found on average 3 copies for wildtype spike mRNA and 4 copies for the mutant one in each VLP (Fig. 1d). As the spike is an envelope protein, we sought to examine if the protein could automatically assemble into the membrane of VLP by Western blot analysis of the lysates of VLP with an integration-defective lentiviral vector (IDLV) as the control (Fig. 1e). We found successful decoration of both with or without proline mutations on the VLPs whereas more mutant spike proteins could be loaded which was in accordance with the RT-qPCR analysis. As glycosylation impacts the immunogenicity and immunodominance of a vaccine[30], we set out to examine the glycosylation status of the spike on the surface of VLPs. Notably, the S2 bands shifted downwards after PNGase F treatment indicating that the spikes on VLPs were modified by N-linked glycosylations mimicking the characteristics of SARS-CoV-2 revealed by the mass spectrometric approach (Fig. 1e)[31].

To examine whether the Spike mRNA in the VLP could be delivered intracellularly in a manner mediated by VSV-G, we transduced 293T cells that were not infected by SARS-CoV-2 unless supplemented with hACE2[32], and then harvested the cells 36 h postinfection for Western blot (Fig. 1f). We found two major bands for spikes which were likely glycosylated full-length singlet spikes and their dimeric/trimeric forms (Fig. 1f). Additionally, we confirmed efficient delivery of spike to 293T cells by confocal analysis (Fig. 1g). From Western blot and confocal microscopy, we consistently observed more spike-mut antigens were delivered by VLP, we therefore chose the mutant spike for in vivo evaluation.

As the mRNA transcribed in vitro for LNP delivery is recognized by intracellular RNA sensors unless chemically modified[33,34], we examined the innate immune property of the VLP-carrying mRNA. Using THP-1 derived macrophages as a model of nucleic acids sensing, we found no significant changes of the type I interferon (IFN) and IFN-stimulated genes ISG-15, and retinoic acid-inducible gene I (RIG-I) (Fig. 1h-j), suggesting that spike mRNA in the VLP was not immunogenic which could be explained by the fact that it was produced intracellularly and shared same modifications as any other endogenous mRNA.

VLP mRNA induces robust spike-specific and durable antibody responses. To evaluate the potential of VLP-mRNA as a vaccine platform, we vaccinated the C57BL/6J mice (n=6 for each group) with VLP carrying mutant spike mRNA (VLP S-mut) via footpad (Fig. 2a). Two weeks later, we performed an enzyme-linked immunosorbent assay (ELISA) using the sera from mice to get access to the spike-specific IgG. As shown in Fig. 2b, we observed significant elicitation of the spike-specific IgG. To evaluate the level of neutralizing antibodies, we performed the neutralizing assay using spike pseudotyped HIV which encodes firefly luciferase - a well-established pseudovirus neutralization assay[35] and found a single injection of VLP S-mut was sufficient to induce potent neutralizing immune responses (Fig. 2c). To confirm the neutralizing activity of vaccinated sera, we adopted the spike pseudotyped lentiviral vector which encodes GFP to transduce Huh-7 cells. We found pre-incubation with 1:40 diluted sera from vaccinated mice almost completely abolished the fluorescence whereas the transduction for VSV-G pseudotyped lentivirus was not apparently affected indicating the spike-specific neutralizing activity (Fig. 2d). Importantly, induction of antibodies with high neutralization titers was demonstrated using live SARS-CoV-2 with an average EC50 titer of 1319 (Fig. 2e). Additionally, we analysed the neutralizing activity of the VLP mRNA vaccine against the B.1.617.2 strain pseudovirus, which showed no significant reduction in the EC50 titer compared to the wildtype strain (Fig. 2f).

To evaluate dynamic changes of VLP mRNA-induced spike-specific antibodies, we performed a short-term follow-up starting from 1 day post-vaccination and a long-term follow-up up to 9 months after vaccination. We found the spike-specific IgG was significantly enhanced on day 7, but was not evident on day 1, 3, and 5 (Fig. 2g). In the long-term follow-up, we found a single dose vaccination induced a durable spike-specific IgG response which was maintained at a high level up to 36 weeks post-immunization (Fig. 2f). Notably, no weight loss was found during the course of vaccination suggesting the safety of VLP-mRNA vaccination (Supplementary Fig. 1). Interestingly, administration of VLP-mRNA via intranasal route elicited spike-specific IgA in the lung, suggesting that this vaccine platform may also be used as an intranasal vaccine to induce mucosal immunity to block the SARS-CoV-2 infection at the first contact site (Supplementary Fig. 2).

Linear epitope landscape in the VLP mRNA vaccinated mice. To dissect the linear epitope profiles of the spike-specific antibodies in the VLP mRNA vaccinated mice, we used a peptide microarray which contains short peptides covering the full-length of spike[36-38]. We found varying intensities of signals corresponding to certain spike peptides for the vaccinated group while no signal was observed for the placebo-treated mice (Fig. 3a). Next, we quantified the signal intensity for antibodies against the S1 domain and receptor-binding domain (RBD), respectively, and found the sera from vaccinated mice elicited significantly higher signals for both domains suggesting the presence of high amounts of S1 and RBD specific IgG in vaccinated mice (Fig. 3b).

To access the panorama of epitopes, we made a heat map for all the 6 vaccinated mice (Fig. 3c and Supplementary Table 1). We found five linear epitopes (S1-55, 57, 60, 76 and 88) located on RBD which is the domain responsible for the host receptor recognition, revealing the key linear motifs on the RBD that are susceptible to specific antibodies (Fig. 3c). More specifically, linear epitope S1-76 located on the center of RBM (receptor binding motif) is the direct binding interface with hACE2. Notably, although the identified epitopes were overall highly diverse, we also found three epitopes, i.e. S2-22, S2-76, and S2-83, were shared by 66.7% of the vaccinated mice. Interestingly, the S2-22 epitope also appeared in the majority of the convalescents uncovered by the peptide microarray[36]. Moreover, the S2-76 and S2-83 epitopes are conserved epitopes among different coronaviruses (Supplementary Fig. 3). Particularly, the S2-83 epitope from the heptad repeat 2 (HR2) region is expected to undergo dramatic structural refolding upon receptor activation, leading to the formation of a six-helix bundle structure that finally drives membrane fusion (Fig. 3d and e).

DC-targeting VLP mRNA elicited a stronger immune response in *vivo*. To target VLP specifically to DC, we used an engineered Sindbis virus glycoprotein (designated SV-G) which recognized the DC-SIGN, a surface protein of DC, to replace the broad tropic VSV-G (Fig. 3a). Next, we verified the tropism of SV-G pseudotyped VLP in vitro by transducing DC2.4 and HeLa cells with 100 ng p24 SV-G VLP-GFP or VSV-G VLP-GFP. Cells were harvested at 48 h post-infection and analyzed by flow cytometry. SV-G VLP efficiently transduced DCs (63% GFP+ cells) whereas only 22.8% in non-DCs (HeLa cells) in contrast to the VSV-G VLP, indicating that SV-G is preferably transducing DCs (Fig. 3b). Next, we assessed and compared the humoral and cellular immune responses of SV-G and VSV-G pseudotyped VLP in vivo (Fig. 3c). Six-week-old C57BL/6 mice (n=4) were immunized 2 μg p24 SV-G VLP-GFP or VSV-G VLP via footpad injection. Humoral immune responses were evaluated at 14 days post-immunization by ELISA. We found the DC-specific SV-G VLP significantly enhanced the level of spike-specific IgG by nearly 1 magnitude (Fig. 3d). Interestingly, the level of p24-specific IgG for SV-G VLP was lower compared to VSV-G (Fig. 3e). Furthermore, we set out to evaluate the spike-specific T cell responses for both the DC-targeting and the non-targeting VLP mRNA and found both elicited strong T cell immune response as shown by the IFN-γ, TNF-α and IL-6 enzyme-linked immunosorbent spot (ELISPOT) assays after stimulating splenocytes with a spike-peptide pool (Fig. 3f-h). Notably, SV-G VLP mRNA vaccination showed averagely more spot forming units (SFUs), although the difference between the two pseudotypes was insignificant (Fig. 3f-h).

DC-targeting VLP mRNA vaccine protected hACE2 mice from the SARS-CoV-2 challenge. To evaluate whether the DC-targeting VLP mRNA vaccine is able to protect mice from live SARS-CoV-2, we challenged hACE2 transgenic mice with live SARS-CoV-2. To acquire optimal efficacy, hACE2 transgenic mice (n = 6 per group) were dosed twice each with 1.5 μg p24 VLP mRNA vaccine (Fig. 5a). The mice were then inoculated by intranasal infection of 10^5 p.f.u SARS-CoV-2 (BetaCoV/Wuhan/WIV04/2019) two weeks after boost vaccination. We detected strong anti-SARS-CoV-2 neutralization antibodies at day 28 with a mean EC50 value of 2643 (Fig. 5b). The weight of mice was monitored daily before euthanasia 3 days post-challenge. We found vaccinated mice keep growing in contrast to the unvaccinated mice which lost 2% weight on average (Fig. 5c). Next, we analyzed the viral RNA levels and found significantly reduction of viral loads in the lung and trachea of vaccinated mice (Fig. 5d and 5e).

To analyse the efficacy of VLP mRNA vaccination on lung protection, we conducted immunofluorescence microscopy which showed the SARS-CoV-2 was hardly detectible in the lung

of vaccinated mice in contrast to the mock vaccinated mice (Fig. 5f). Moreover, we performed hematoxylin and eosin (HE) staining to analyse the pathology SARS-CoV-2 infected mice, which showed that the control mice had alveolar epithelial cell hyperplasia, local pulmonary alveoli shrank and infiltration of inflammatory cells in lung interval (Fig. 5g). In contrast, vaccinated mice showed attenuation of the inflammatory response with only mild perivascular and alveolar infiltration of inflammatory cells observed in very few areas (Fig. 5g). Together, these results indicate that the DC-targeting VLP mRNA vaccine mediated efficient protection against live SARS-CoV-2 infection and prevented the inflammatory reaction.

DC-targeting VLP mRNA vaccine protected mice from the HSV-1 challenge. To evaluate the flexibility of VLP mRNA as a vaccine platform, we designed an HSV-1 VLP mRNA vaccine by incorporating HSV-1 gB and gD mRNA into the SV-G pseudotyped VLP (Fig. 6a). 14 days after the prime-boost vaccination, the depilated mice were challenged with 10^7 p.f.u of HSV-1 17 syn+ in the format of 10 μL on the abraded skin (Fig. 6b). Prime vaccination significantly induced the neutralizing IgG against HSV-1 while the second vaccination further boost the neutralizing antibody titers by 4-fold (Fig. 6c). Interestingly, although the gB and gD antigens were derived from HSV-1, we detected cross-neutralizing activity against HSV-2, suggesting the vaccine might also be functional against HSV-2 infection (Fig. 6d). After challenging the skin with live HSV-1, we found vaccinated mice did not show typical symptoms of disease progression (n = 4) in contrast to the mock-treated mice which showed mild zosteriform lesions at 2 d.p.i and hunched posture, abnormal gait and severe zosteriform lesions at 6 d.p.i (Fig 6e).

To evaluate whether this vaccine blocked the transmission of HSV-1 from the skin to the peripheral nervous system, the skin and dorsal root ganglion (DRG) samples were collected at the time of euthanasia and examined for the HSV-1 genome. The viral load was significantly reduced in the skin tissues of the vaccinated group by plaque assay and viral genome analysis, respectively (Fig. 6f-g). Remarkably, we found an almost undetectable level of viral loads in the DRG of vaccinated mice by both assays indicating the strong neuronal protection by VLP mRNA vaccination (Fig. 6h-i). To get access into the tissue structure after vaccination and virus challenge, we conducted HE staining of the skin which was found well preserved in the vaccinated group while the unvaccinated mice showed thickened epidermis and seriously damaged dermis (Fig. 6j). Next, we performed immunohistochemistry (IHC) to compare the local immune response in the skin of infected mice and found apparent CD4+ cells enrichment, but not CD8+ cells, in the skin of unvaccinated mice after the HSV-1 challenge. Additionally, a large number of neutrophils infiltrated the dermis of the

unvaccinated mice, which was not evident for vaccinated mice and non-infected controls. Taken together, the DC-targeting VLP mRNA vaccine effectively protected mice from live HSV-1 infection.

Discussion

Currently, there are still no effective vaccines available for several infectious diseases such as HSV-1, HSV-2 and HIV and non-infectious diseases including most cancers. Dendritic cells are the most potent antigen-presenting cells and an important cell type to induce effective and durably protective T cell immunity as well as the humoral immune response to block pathogens or attack cancer cells[39]. The clinically approved mRNA vaccines are based on LNP which is internalized passively by diverse somatic cells including muscle cells, B cells, CD4+ T cells and tissue-resident or recruited APCs[17]. The alternative is to deliver mRNA vaccine specifically to DCs. In this study, we developed a DC-targeting mRNA vaccine platform by incorporating mRNA into VLP and decorating its surface with an engineered Sindbis virus envelope. We found the DC-targeting VLP mRNA vaccine induced durable IgG response and strong T cell immunity. Moreover, the VLP mRNA vaccines are capable of protecting mice from virus infection in both live SARS-CoV-2 and HSV-1 infection models.

Our VLP is derived from the lentiviral vector. LV has been reported to induce both strong and long-lasting cellular and humoral immune responses[40]. Moreover, LV is negligibly inflammatory and absent of pre-existing vector-specific immunity in most humans unlike many other viral vectors[40]. Additionally, LV can be re-targeted to DC by surface engineering. For these advantages, LV has been used in clinical trials against HIV and cancers[41,42]. Recently, LV has been administrated intranasally in preclinical animal models and showed efficient protection against SARS-CoV-2 infection[43]. Even with the remarkable progresses, LV faces two internal challenges, 1) the viral DNA possesses insertional risks, 2) the existence of SAMHD1, a cellular enzyme that depletes intracellular deoxynucleoside triphosphates and blocks reverse transcription, may limit the antigen presentation[44]. While VLP keeps the advantages of LV, it delivers mRNA which is absent of insertional mutagenesis. Also, no reverse transcription step is involved, therefore, escaping the negative control of SAMHD1.

Targeting DC has been deemed as an attractive strategy to improve the effectiveness of current vaccine technologies. In the past decade, over 100 preclinical studies have analysed DC-targeting approaches and their effectiveness to induce T cell and antibody responses[39]. Yet, it remains unclear

whether DC-targeting vaccines will be superior to non-specific vaccines. Our study showed DC-targeting VLP mRNA induced nearly 1 magnitude higher spike-specific IgG than the broad tropic VSV-G pseudotyped counterpart. Although DC-specific VLP mRNA induced averagely higher level of spike-specific T cell response, the difference was insignificant compared to VSV-G, possibly due to VSV-G entering into DC very efficiently or depending on antigens[42].

The future applications of the VLP-based mRNA vaccine include as an in situ DC vaccine to cure cancers in combination with immune checkpoint inhibitors or being used a therapeutic vaccine to remove the established viral infections such as HBV and HPV. Furthermore, the potency of VLP mRNA vaccine may further be improved by combining circular RNA or self-amplifying RNA which may extend the persistence of antigen expression and lower the necessary dose for vaccination, therefore, improving the efficacy while downregulating the cost.

Methods

Cell cultures

293T, Hela, Huh-7, DC2.4, Vero and Vero E6 cells were cultured in DMEM (Gibco, USA) supplemented with 10% fetal bovine serum (Gibco, USA) and 1% penicillin/streptomycin (P/S) (Thermo Fisher Scientific, USA). Primary splenocytes, mouse glia cells and THP-1 cells were cultured in RPMI 1640 (Gibco, USA) with 10% fetal bovine serum. THP-1 cells were differentiated into macrophage-like cells with 150 nM phorbol 12-myristate 13-acetate (PMA) (Sigma) before the experiment.

Plasmids

pCCL-PGK-spike-flag and pCCL-PGK-spike-mut-flag were constructed by replacing the GFP gene in pCCL-PGK-eGFP with spike or mutant spike (K1003P and V1004P) gene. pCMV-spike-mut-6XMS2, pCMV-spike-6XMS2-flag, pCMV-spike-mut-6XMS2-flag and pCMV-gB1-gD1-6XMS2 were generated by inserting 6XMS2 stem-loop repeats between the stop codon of spike (or mutant spike, or gB1gD1 gene) and the polyA sequence while the whole expression cassette is under the control of CMV promoter.

Production of VLP, IDLV, and pseudovirus

VLP, IDLV, and pseudovirus were produced by 293T cells in 15-cm dishes. Cells were seeded in the 15-cm dish at a density of 1.35×10^7/dish 24 h before calcium phosphate transfection. The media

were refreshed 12 h after transfection. 48 h and 72 h post-transfection, supernatants were filtered through a 0.45-μm filter (Millipore) and ultracentrifuged at 4°C for 2 h. Pellets were re-suspended in PBS and stored at −80°C. To produce GFP-expressing spike pseudovirus and IDLV (IDLV-spike or IDLV-spike-mut), cells were transfected with 9.07 μg pMD.2G (or corresponding spike plasmids), 7.26 μg pRSV-Rev, 31.46 μg pMDlg/pRRE-D64V, 31.46 μg pCCL-PGK-eGFP (or pCCL-PGK-spike-flag or pCCL-PGK-spike-mut-flag). To produce VLP-spike and VLP-spike-mut (or SV-G VLP), cells were transfected with 9.07 μg pMD.2G (or pCMV-SV-G-mut), 7.26 μg pRSV-Rev, 15.73μg pMDlg/pRRE-D64V, 15.73 μg pMS2M-PH-gagpol-D64V, 31.46 μg pCMV-spike-6XMS2, or pCMV-spike-mut-6XMS2, or their flag versions. To produce luciferase-encoding spike (or B1.617.2 spike) pseudovirus, 293T cells were transfected with 20 μg pcDNA3.1-SARS-Cov2-spike (or pcDNA3.1-SARS-Cov2-B1.617.2 spike) and 20 μg pNL4-3.luc.RE.

Western blot

To detect spike protein associated with VLP or IDLV, Western Blot was performed to detect spike protein with/without treatment of PNGase F (NEB). 100 ng p24 particles were incubated with Glycoprotein Denaturing Buffer at 98°C for 10 min. After adding GlycoBuffer 2 and NP-40 (10%), the mixtures were incubated with/without PNGase F at 37°C for 2 h. Mixtures were then incubated with SDS loading buffer (Beyotime Biotechnology) before sample loading. To detect spike protein expressed in cells, 293T cells were lysed in RIPA 36 h after being transduced with VLP or IDLV. The lysates were incubated with SDS loading buffer supplemented with 2.5% β-Mercaptoethanol at 37°C for 30 min without boiling. The proteins were separated by SDS-polyacrylamide gel electrophoresis and transferred to the PVDF membrane. The membrane was blocked by 5% fat-free milk dissolved in TBS/0.05% Tween-20 for 1 h. The membrane was cut according to the marker and incubated with anti-flag monoclonal antibody (Sigma) overnight at 4°C. The membranes were incubated with anti-mouse secondary antibodies (Cell Signaling Technology) for 1 h at room temperature. Proteins were visualized by hypersensitive ECL chemiluminescence (Beyotime Biotechnology).

Quantitative PCR

To detect spike mRNA numbers carried by VLP, total RNAs from all samples were extracted using the Viral DNA/RNA extraction kit (TaKaRa) followed by cDNA synthesization using the HiScript Q RT SuperMix for qPCR (Vazyme Biotech Co,. Lot) according to the manufacturer's protocol.

RT-qPCR was performed using qPCR SYBR Green Master Mix (Vazyme Biotech Co,. Lot) following the manufacturer's protocol. Plasmid pLV-PGK-S-mut diluted into copies of 10^3, 10^4, 10^5, 10^6, 10^7 per microliter were used to make a standard curve for absolute quantification. Primer sequences are as follows, forward primer: 5'-ACAGATGAGATGATCGCCCAG-3', reverse primer: 5'-TCTGCATGGCGAAAGGGATC-3'. To analysis viral RNA in tissues. Total Lung sample RNAs were extracted using TRIzol reagent (Vazyme Biotech Co,. Lot) according to the manufacturer's protocol. The SARS-Cov-2 viral load was determined following reverse transcription. The product was performed using qPCR SYBR Green Master Mix (Vazyme Biotech Co,. Lot). To quantify HSV-1 genomes in mouse skin or neural tissue, genomic DNA and viral DNA were extracted and subjected to qPCR to detect HSV-1 (forward primer: 5'-TACAACCTGACCATCGCTTG-3', reverse primer: 5'-GCCCCCAGAGACTTGTTGTA-3'), which was then normalized to mouse *Gapdh* (forward primer: 5'-GTGTTCCTACCCCCAATGTG-3', reverse primer: 5'-TAGCCCAAGATGCCCTTCAG-3').

Mice

6-8 weeks old, male, specific-pathogen-free (SPF) C57BL/6 mice or hACE2 transgenic mice were inoculated with VLP, IDLV, or PBS by foot-pad injection. Animals were sacrificed by cervical dislocation under isoflurane. The animal study has complied with the guidelines of the Institutional Animal Care and Use Committee (IACUC) of the Shanghai Jiao Tong University.

ELISA

HIV p24 ELISA (Biodragon Immunotechnologies) was used to measure the p24 level of the lentiviral particles according to the manufacturer. To detect SARS-CoV-2-spike specific antibodies *in vivo*, sera from the animals were used to test the spike-specific IgG by Mouse IgG ELISA (Bethyl) with a few modifications. 200 ng recombinant spike or p24 proteins (Novoprotein) were coated in 96-well ELISA plates overnight at 4°C in a carbonating buffer (PH 9.5). The plates were blocked with PBS containing 0.05% Tween 20 (PBS-T) and 1% bovine serum albumin (BSA) for 1 h. Sera samples were diluted 1:4 using PBS and incubated for 2 h before washing following the manufacturer's instructions.

ELISPOT assay

To find the involvement of cellular immunity, the cytokine production in the splenic cells upon treatment with spike peptides in vitro was measured. Spleens were removed aseptically, placed in the RPM 1640 medium, gently homogenized, and passed through the cell strainer (Jet Bio-Filtration) to generate a single-cell suspension. Erythrocytes were rapidly washed and lysed by the RBC lysis buffer (Sangon Biotech), and the splenocytes were resuspended in 1 mL RPMI 1640 medium. 5×10^5 splenocytes were seeded in anti-mouse IFN-γ, IL-6 and TNF-α antibody precoated ELISPOT plates (Mabtech). Cells were incubated with a pool of SARS-CoV-2 spike peptides (15-mer peptides with 11-amino acid overlap covering the entire spike protein; GenScript) of 0.2 μg/well for each peptide for 36 h, or 2 μg/mL concanavalin A (ConA) (Sigma) and culture medium as controls. The detection procedure was conducted according to the manufacturer's instructions. Spots were counted and analyzed by using Mabtech IRIS FluoroSpot/ELISpot reader.

Neutralization assay

To determine the serum neutralization activity against GFP-expressing spike pseudovirus. Vaccinated mouse serum (40×dilutions) were incubated with GFP-expressing spike pseudovirus at 37°C for 1 h before adding the mixtures to Huh-7 cells (4×10^4 cells per well in 48-well plates). The media were changed after 12 h and photos were taken at 48 h post-infection. For luciferase-encoding spike pseudovirus and SARS-CoV-2 delta strain pseudovirus neutralization assay. Serial dilutions of VLP mRNA or placebo vaccinated mouse serum were incubated with pseudovirus at 37°C for 1 h before adding to Huh-7 cells (10^4 cells per well in 96-well plates). The culture media were refreshed 12 h post-infection, which was followed by an additional 48 h incubation. Huh-7 cells were subsequently lysed with 50 μL lysis reagent (Promega), and 30 μL lysates were transferred to 96-well Costar flat-bottom luminometer plates (Corning Costar) for the detection of relative light units using the Firefly Luciferase Assay Kit (Promega) with an Ultra 384 luminometer (Tecan). A nonlinear regression analysis was performed on the resulting curves using Prism (GraphPad) to calculate half-maximal inhibitory concentration (EC50) values. Neutralization assays with live SARS-CoV-2 (USA-WA1/2020) were performed in a biosafety level 3 (BSL3) facility with strict adherence to institutional regulations. Serum samples were heat-inactivated and tested at a starting dilution of 1:20 and were serially diluted 2-fold up to the final dilution of 1:10240. After serum incubation with 40 p.f.u of SARS-CoV-2 for 1 h at 37°C, the virus serum mixtures were added onto Vero E6 cell monolayers. Supernatants were replaced with 1% low melting-point agar (Sangon Biotech) in DMEM with 2% FBS and 1% penicillin-streptomycin 1 h post-infection. The

plates were fixed and stained after 3 days of culture for the number plaques. The HSV-1 and HSV2 neutralizing antibody titers were tested at a starting dilution of 1:10 and were serially diluted 2-fold up to the final dilution of 1:1280. After serum incubation with 50 p.f.u of HSV-1 or HSV-2 for 1 h at 37°C, the mixtures were added to Vero cell for 1 h and replaced with 1% low melting-point agar in DMEM.

Immunofluorescence imaging

293T cells were seeded to 48-well plates with 0.1 mg/mL poly-D-lysine coated cover glasses at a destiny of 4×10^4/well. On the next day, cells were transduced by 150 ng IDLVs or VLPs, or transfected by 0.6 μg pCMV-spike-6XMS2 or pCMV-spike-mut-6XMS2 plasmids. Cells were fixed using 4% paraformaldehyde 36 h after transduction and transfection. Cells were then stained by anti-flag tag antibody (Proteintech) followed by Alexa Fluor 555 IgG incubation (Cell Signaling Technology) and nuclei staining with DAPI (Beyotime Biotechnology). To evaluate SARS-Cov-2 distribution in lung tissues. The lungs of mice were fixed in 4% PFA overnight at 4 °C before transferring to 30% sucrose, then embedded with optimal cutting temperature (OCT). Sections were stained with SARS-CoV-2 NP antibody. The imaging was performed on a confocal microscope (A1Si, Nikon) to verify the expression of Spike proteins.

SARS-CoV-2 challenges in hACE2 transgenic mice

6-8 weeks old hACE2 transgenic mice were inoculated with VLP mRNA (1.5 μg p24, n=6) or PBS by footpad injection, and boosted at day 14 (1.5 μg p24). Mice were challenged with 10^5 TCID50 of SARS-CoV-2 via intranasal administration at day 28 post-immunization. Three-days post challenge, all mice were sacrificed for tissue pathological and virological analyses.

Histopathology

Lung tissues were fixed in 4% formaldehyde and embedded in paraffin. Lung or skin sections were stained with hematoxylin and eosin and analyzed for tissue status. For immunohistochemistry, the sections were treated with 3% hydrogen peroxide for 25 min to block endogenous peroxidase activity. The sections were then blocked with 3% BSA at room temperature for 30 min and incubated with anti-CD4 (1:100; Servicebio, gb13064) or anti-CD8 (1:1,000; Servicebio, gb11068) at 4 °C overnight. Then sections were then incubated with an anti-rabbit secondary antibody (1:500; Servicebio, gb23303), followed by incubation with freshly prepared DAB substrate solution to

detect the antibody. Sections were counterstained with hematoxylin, blued with ammonia water, and then dehydrated and coverslipped.

Plaque assay

To quantify infectious SARS-CoV-2 particles in lung, endpoint titrations were performed on confluent Vero E6 cells. Lung homogenates were serially diluted in DMEM supplemented with 2% FBS and 1% penicillin-streptomycin and incubated on cells for 2 h at 37°C. Then, the supernatants were replaced with 1% low melting-point agar in DMEM with 2% FBS and 1% penicillin-streptomycin. The plates were inverted and incubated at 37°C for 3 days. Plates were fixed with 4% PFA for 10 min at room temperature and then stained with 1ml 1% crystal violet for 1.5 hours. Plaques were counted manually to determine the infectious virus titer. HSV-1 and HSV-2 titers were performed on confluent Vero cells. The viral load was calculated based on the count of plaques and dilution factor.

HSV-1 challenges in mice

6-8 weeks old mice (n=4) were inoculated with VLP-gB1-gD1 (1.5 μg p24) or PBS by footpad injection, and boost at day 14 (1.5 ug P24). At day 14 post boost immunization, mice were depilated and abraded with a disposable emory board, then challenged with 10^7 p.f.u of HSV-1 17 syn+ in 10 μL deposited on the abraded skin. Sera were collected for the neutralization assay. Skin graphs were collected at the indicated times after infection. 6 days after HSV-1 infection, mouse skin was processed for H&E, plaque assay or DNA isolation.

Statistics

Data are presented as mean ± s.e.m. in all experiments. One-way analysis of variance (ANOVA) or student's t-tests were performed to determine the P values. *indicates statistical significance (*P< 0.05, **P< 0.01, ***P< 0.001; n.s.=non-significant).

Data availability

Data generated or analysed during this study are available from the corresponding author on reasonable request.

Acknowledgement

Y.C. is supported by National Natural Science Foundation of China [31971364], Pujiang Talent Project of Shanghai [GJ4150006], and Startup funding from Shanghai Center for Systems Biomedicine, Shanghai Jiao Tong University [WF220441504]. J.H. is supported by the National Natural Science Foundation of China [81970766 and 82171102] and the Shanghai Innovation Development Program [2020-RGZN-02033]. T.Y. is supported by the National Key R&D Program of China [2019YFA0904400] and National Natural Science Foundation of China [81822027, 81630090]. S. T. is supported by National Natural Science Foundation of China [No. 31970130] and the National Key R&D Program of China [2020YFE0202200].

Conflict of interest

Y.C. is a consultant and co-founder of BDgene Therapeutics. X.W. is current employee of BDgene Therapeutics.

Author contribution

D.Y, S.L. and Y.C. conceived the study and designed the experiments; D.Y., S.L., X.T, Y.L., Z.X., J.H., X.Z., X.W., and J.H. performed the experiments; all the authors analysed the data; D.Y., S.L., and Y.C. wrote the manuscript with the help from all the authors.

References

1. Roth, G.A., *et al.* Designing spatial and temporal control of vaccine responses. *Nat Rev Mater*, 1-22 (2021).
2. Colby, D.J., *et al.* Safety and immunogenicity of Ad26 and MVA vaccines in acutely treated HIV and effect on viral rebound after antiretroviral therapy interruption. *Nat. Med.* **26**, 498-501 (2020).
3. Ng'uni, T., Chasara, C. & Ndhlovu, Z.M. Major Scientific Hurdles in HIV Vaccine Development: Historical Perspective and Future Directions. *Front Immunol* **11**, 590780 (2020).
4. Bernstein, D.I., *et al.* The R2 non-neuroinvasive HSV-1 vaccine affords protection from genital HSV-2 infections in a guinea pig model. *NPJ Vaccines* **5**, 104 (2020).
5. Awasthi, S., *et al.* Nucleoside-modified mRNA encoding HSV-2 glycoproteins C, D, and E prevents clinical and subclinical genital herpes. *Science Immunology* **4**, eaaw7083 (2019).
6. Wang, W., *et al.* Dual-targeting nanoparticle vaccine elicits a therapeutic antibody response against chronic hepatitis B. *Nat Nanotechnol* **15**, 406-416 (2020).
7. Roden, R.B.S. & Stern, P.L. Opportunities and challenges for human papillomavirus vaccination in cancer. *Nat. Rev. Cancer* **18**, 240-254 (2018).
8. Sahin, U., *et al.* Personalized RNA mutanome vaccines mobilize poly-specific therapeutic immunity against cancer. *Nature* **547**, 222-226 (2017).
9. Keskin, D.B., *et al.* Neoantigen vaccine generates intratumoral T cell responses in phase Ib glioblastoma trial. *Nature* **565**, 234-239 (2019).
10. Zhu, N., *et al.* A Novel Coronavirus from Patients with Pneumonia in China, 2019. *N. Engl. J. Med.* (2020).
11. Polack, F.P., *et al.* Safety and Efficacy of the BNT162b2 mRNA Covid-19 Vaccine. *N. Engl. J. Med.* **383**, 2603-2615 (2020).
12. Baden, L.R., *et al.* Efficacy and Safety of the mRNA-1273 SARS-CoV-2 Vaccine. *N. Engl. J. Med.* **384**, 403-416 (2021).
13. Widge, A.T., *et al.* Durability of Responses after SARS-CoV-2 mRNA-1273 Vaccination. *N. Engl. J. Med.* **384**, 80-82 (2021).
14. Thomas, S.J., *et al.* Safety and Efficacy of the BNT162b2 mRNA Covid-19 Vaccine through 6 Months. *N. Engl. J. Med.* (2021).
15. Tenforde, M.W., *et al.* Effectiveness of SARS-CoV-2 mRNA Vaccines for Preventing Covid-19 Hospitalizations in the United States. *medRxiv* (2021).
16. Wang, Y., *et al.* mRNA vaccine: a potential therapeutic strategy. *Mol. Cancer* **20**, 33 (2021).
17. Lindsay, K.E., *et al.* Visualization of early events in mRNA vaccine delivery in non-human primates via PET–CT and near-infrared imaging. *Nature Biomedical Engineering* **3**, 371-380 (2019).
18. Eisenbarth, S.C. Dendritic cell subsets in T cell programming: location dictates function. *Nat. Rev. Immunol.* **19**, 89-103 (2019).
19. Lanzavecchia, A. & Sallusto, F. Regulation of T cell immunity by dendritic cells. *Cell* **106**, 263-266 (2001).
20. Heath, W.R., Kato, Y., Steiner, T.M. & Caminschi, I. Antigen presentation by dendritic cells for B cell activation. *Curr. Opin. Immunol.* **58**, 44-52 (2019).
21. Wykes, M., Pombo, A., Jenkins, C. & MacPherson, G.G. Dendritic cells interact directly with naive B lymphocytes to transfer antigen and initiate class switching in a primary T-dependent response. *J. Immunol.* **161**, 1313-1319 (1998).
22. Igyarto, B.Z., Jacobsen, S. & Ndeupen, S. Future considerations for the mRNA-lipid nanoparticle vaccine platform. *Curr Opin Virol* **48**, 65-72 (2021).

23. Blumenthal, K.G.*, et al.* Delayed Large Local Reactions to mRNA-1273 Vaccine against SARS-CoV-2. *N. Engl. J. Med.* **384**, 1273-1277 (2021).
24. Yu, Y.*, et al.* Antibody-dependent cellular cytotoxicity response to SARS-CoV-2 in COVID-19 patients. *Signal Transduct Target Ther* **6**, 346 (2021).
25. Yang, L.*, et al.* Engineered lentivector targeting of dendritic cells for in vivo immunization. *Nat. Biotechnol.* **26**, 326-334 (2008).
26. Wrapp, D.*, et al.* Cryo-EM structure of the 2019-nCoV spike in the prefusion conformation. *Science*, eabb2507 (2020).
27. Yin, D.*, et al.* Targeting herpes simplex virus with CRISPR-Cas9 cures herpetic stromal keratitis in mice. *Nat. Biotechnol.* **39**, 567-577 (2021).
28. Ling, S.*, et al.* Lentiviral delivery of co-packaged Cas9 mRNA and a Vegfa-targeting guide RNA prevents wet age-related macular degeneration in mice. *Nat Biomed Eng* **5**, 144-156 (2021).
29. Hu, B., Tai, A. & Wang, P. Immunization delivered by lentiviral vectors for cancer and infectious diseases. *Immunol. Rev.* **239**, 45-61 (2011).
30. Chang, D. & Zaia, J. Why Glycosylation Matters in Building a Better Flu Vaccine. *Molecular & Cellular Proteomics* **18**, 2348 (2019).
31. Watanabe, Y., Allen, J.D., Wrapp, D., McLellan, J.S. & Crispin, M. Site-specific glycan analysis of the SARS-CoV-2 spike. *Science*, eabb9983 (2020).
32. Crawford, K.H.D.*, et al.* Protocol and reagents for pseudotyping lentiviral particles with SARS-CoV-2 Spike protein for neutralization assays. *bioRxiv*, 2020.2004.2020.051219 (2020).
33. Wienert, B., Shin, J., Zelin, E., Pestal, K. & Corn, J.E. In vitro-transcribed guide RNAs trigger an innate immune response via the RIG-I pathway. *PLoS Biol.* **16**, e2005840 (2018).
34. Mu, X., Greenwald, E., Ahmad, S. & Hur, S. An origin of the immunogenicity of in vitro transcribed RNA. *Nucleic Acids Res.* **46**, 5239-5249 (2018).
35. Ying, T.*, et al.* Exceptionally Potent Neutralization of Middle East Respiratory Syndrome Coronavirus by Human Monoclonal Antibodies. *J. Virol.* **88**, 7796 (2014).
36. Ma, M.L.*, et al.* Systematic profiling of SARS-CoV-2-specific IgG responses elicited by an inactivated virus vaccine identifies peptides and proteins for predicting vaccination efficacy. *Cell Discov* **7**, 67 (2021).
37. Jiang, H.W.*, et al.* SARS-CoV-2 proteome microarray for global profiling of COVID-19 specific IgG and IgM responses. *Nat. Commun.* **11**, 3581 (2020).
38. Li, Y.*, et al.* Linear epitope landscape of the SARS-CoV-2 Spike protein constructed from 1,051 COVID-19 patients. *Cell Rep* **34**, 108915 (2021).
39. Kastenmuller, W., Kastenmuller, K., Kurts, C. & Seder, R.A. Dendritic cell-targeted vaccines--hope or hype? *Nat. Rev. Immunol.* **14**, 705-711 (2014).
40. Ku, M.-W., Charneau, P. & Majlessi, L. Use of lentiviral vectors in vaccination. *Expert Rev. Vaccines*, 1-16 (2021).
41. Pollack, S.M.*, et al.* First-in-Human Treatment With a Dendritic Cell-targeting Lentiviral Vector-expressing NY-ESO-1, LV305, Induces Deep, Durable Response in Refractory Metastatic Synovial Sarcoma Patient. *J. Immunother.* **40**, 302-306 (2017).
42. Ku, M.W.*, et al.* Lentiviral vector induces high-quality memory T cells via dendritic cells transduction. *Commun Biol* **4**, 713 (2021).
43. Ku, M.-W.*, et al.* Intranasal vaccination with a lentiviral vector protects against SARS-CoV-2 in preclinical animal models. *Cell Host Microbe* (2020).
44. Norton, T.D. & Miller, E.A. Recent Advances in Lentiviral Vaccines for HIV-1 Infection. *Front Immunol* **7**, 243 (2016).

Legends

Figure 1. Design and characterization of VLP-based SARS-CoV-2 mRNA vaccine. a, Construction of mRNA-encoding plasmid which transcribes a MS2 stem loop-containing spike mRNA. The spike mRNA and protein will be packaged into VLP via the RNA-coat protein interaction and self-assembly, respectively. NTD, N-terminal domain; RBD, receptor binding domain; SD1 and SD2, subdomain 1 and 2; FP, fusion peptide; HR1 and HR2, heptad repeat 1 and 2; TM, transmembrane domain; CT, cytoplasmic tail. **b**, Schematic illustration of the production process of the SARS-CoV-2 vaccine using VLP platform. **c**, Electron microscopy image of VLP. Scale bar, 100 nm. **d**, Copy number of spike mRNA in each VLP particle. The copy number was detected by absolute quantification RT-qPCR and normalized to IDLV S-mut (2 copies RNA per virion). **e**, Western blot analysis of the spike protein in the virion treated with/without PNGase F. IDLV use as a control. 100 ng p24 for each vector. **f**, Western blot analysis of the spike protein expression. 293T cells were collected 36 h after transfection or transduction. 300 ng p24 virus or VLP used for each well. **g**. Confocal analysis of spike protein expression. 293T cells were fixed 36 h after transfection or transduction. Images are representative of three independent biological replicates in one experiment. **h**-**j**, Innate immune response induced by VLP in THP-1 derived macrophages. Cells were harvested for IFNB1, ISG15 and RIG-I analysis by RT-qPCR 6 h after transduction. 150 ng p24 per well for IDLV S-mut or VLP S-mut. 1.5 μg poly I:C per well as positive controls. ***P< 0.0001 (**h**-**j**). S represents spike. S-mut represents mutant spike. Data and error bars represent mean ± s.e.m.; one-way ANOVA with Dunnett's *post hoc* tests were performed; n.s.=non-significant.

Figure 2. VLP mRNA induces robust and durable spike-specific antibody responses. a, Schematic illustration of the working plan (n=5). The sera were collected 14 days after footpad VLP injection for further analysis. **b**, ELISA analysis of spike specific IgG. ***P< 0.0001. **c**-**f**, Neutralization activity of vaccinated sera evaluated by luciferase assay (**c** and **f**), confocal microscopy (**d**) and plaque assay(**e**). A firefly luciferase-encoding pseudovirus, GFP-expressing SARS-CoV-2 pseudovirus and live SARS-CoV-2 (USA-WA1/2020) was used, respectively, to transduce Huh-7 or Vero E6 cells. *P= 0.0260 (**c**). Images are representative of three independent biological replicates in one experiment (**d**). **g** and **h**, Antibody changes in short-term (**g**) and long-term (**h**) follow-up vaccination. Mice were immunized with 1.5 μg VLP S-mut via footpad injection, sera were collected at the indicated time for IgG ELISA. Data and error bars represent

mean ± s.e.m.; unpaired two-tailed student's t-tests (**b** and **c**); two-tailed Wilcoxon matched-pairs signed-rank test (**f**).

Figure 3. Linear epitope landscape in the VLP mRNA vaccinated mice. a, Representative images of spike peptide microarray. S1 protein and RBD were included in the microarray as controls. Highly frequent positive peptides were labeled. **b**. Antibody responses against S1 protein or RBD in vaccinated mice. Signal intensity was averaged fluorescent intensity of tinplated spots for each array. ***P< 0.0001. **c**, Heatmap of antibody responses against peptides. The gray grid indicates a negative response. **d** and **e**, Analysing the epitopes of VLP induced spike-specific antibodies on spike protein. 6 mice were used for each group, 1.5 μg VLP S-mut or 50 μL PBS were injected via footpad into each mouse. Data and error bars represent mean ± s.e.m.; unpaired two-tailed student's t-tests.

Figure 4. DC-targeting VLP-mRNA vaccine induced enhanced spike-specific IgG and T cell immune response. **a**, Illustration of the production process of the DC-specific VLP-mRNA vaccine. **b**, Evaluating the DC-specificity of SV-G pseudotyped VLP. 100 ng p24 GFP mRNA-carrying VLP pseudotyped by SV-G and VSV-G, respectively, were transduced to $4x10^4$ DC 2.4 or HeLa cells. Three days later, the transduction efficiency was measured by flow cytometry analysing the GFP expression. ***P =0.0003 of DC2.4 and ***P< 0.0001 of Hela for SV-G VLP versus VSV-G VLP. **c**, The working plan for analysing VLP mRNA elicited the humoral and cellular immune responses. **d** and **e**, ELISA analysis of spike specific and p24 specific IgG. Serum was collected at 14 days post-immunization (1.5 μg p24 VLP per mouse, n=4 mice). *P = 0.0286 for all groups (**d**). *P = 0.0286 for Mock versus VSV-G and Mock versus SV-G, *P = 0.0571 for VSV-G versus SV-G (**e**). **f**-**h**, Quantification of the number of IFN-γ, TNF-α and IL-6 spot-forming cells isolated from the spleen after stimulation with spike peptide pool. *P = 0.0286 for all groups (**f**-**h**). Representative images of ELISPOT wells showed on left. Images are representative of three independent biological replicates in one experiment. Data and error bars represent mean ± s.e.m.; unpaired two-tailed Mann-Whitney tests (**d**, **e**, **f**-**h**) ; n.s.=non-significant.

Figure 5. DC-specific VLP-mRNA vaccine efficiently protected hACE2 transgenic mice from the SARS-CoV-2 challenge. **a**, Scheme of vaccination and challenge. 1.5 μg p24 SV-G VLP or 50 μL PBS were immunized by footpad injection (n=6), and boosted at 14 days post prime

immunization. Mice were challenged with 10^5 TCID50 of SARS-CoV-2 at 14 days post boost immunization by intranasal administration. All mice were euthanized at 3 d.p.i. **b**, Neutralization activity of vaccinated sera against live SARS-CoV-2 (USA-WA1/2020). **c**, The percentage of mice weight change after infection. **P* = 0.0253. **d** and **e**, Viral loads in lung and trachea detected by RT-qPCR. **f**, Confocal analysis of SARS-CoV-2 in the lung. ***P* = 0.0042 (**d**) and ****P* < 0.0001 (**c**). **g,** Lung histopathology analysis by hematoxylin and eosin (red arrow, inflammatory cell infiltration; blue arrow, alveolar destruction). Each image is a representative of a group of 4 mice (**f** and **g**). Data and error bars represent mean ± s.e.m.; unpaired two-tailed student's t-tests (**c**-**e**).

Figure 6. DC-specific VLP-mRNA co-delivering gB1 and gD1 efficiently protected mice from the HSV-1 infection. **a**, Schematic illustration of the production process of the VLP gB1-gD1 vaccine. **b**, Flowchart for analysing the effectiveness of VLP gB1-gD1 vaccination against HSV-1 infection. Six-week-old C57BL/6 mice (n=4) were immunized with 2 μg p24 VLP mRNA vaccine at day 0 and day 14, respectively. **c** and **d**, Neutralization activity against live HSV-1 and HSV-2. n=4 mice. ***P* = 0.0032 for Prime versus NC, ***P* = 0.0026 for Boost versus NC and **P* = 0.0109 for Prime versus Boost (**c**). **P* = 0.0365 for Prime versus NC, **P* = 0.0309 for Boost versus NC (**d**). **e**, Representative images of skin at 2 d.p.i. and 5 d.p.i. Each image is representative of four mice in one experiment. **f** and **g**, Plaque assay and qPCR analysis of the HSV-1 replication in the skin at 6 d.p.i. **P* = 0.0113 (**f**), **P* = 0.0147 (**g**). **h** and **i**, Plaque assay and qPCR analysis of the HSV-1 replication in the DRG at 6 d.p.i. **P* = 0.0437 (**h**), ***P* = 0.0088 (**i**). **j**, HE analysis of skin histopathology at 6 d.p.i. **k**, IHC analysis of CD4+ and CD8+ T cells infiltration in the skin 6 days after infection. e, epidermis; d, dermis; m, muscle. Each image is a representative of four mice in one experiment (**e, j** and **k**). Data and error bars represent mean ± s.e.m.; unpaired two-tailed Student's t-tests (**c**, **d**, **f**- **i**); n.s.=non-significant.

Figures

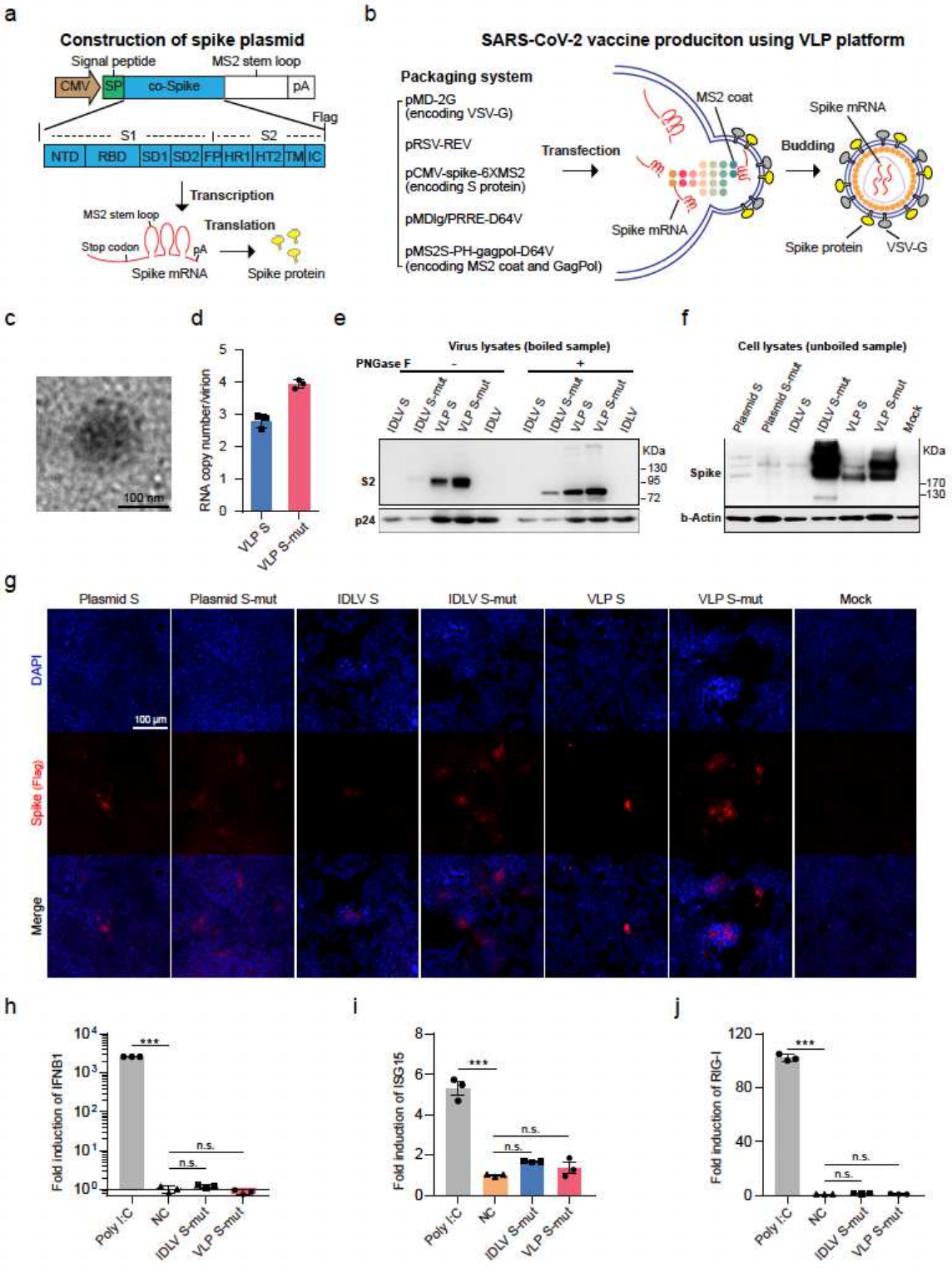

Figure 1

Design and characterization of VLP-based SARS-CoV-2 mRNA vaccine. a, Construction of mRNA-encoding plasmid which transcribes a MS2 stem loop-containing spike mRNA. The spike mRNA and protein will be packaged into VLP via the RNA-coat protein interaction and self-assembly, respectively.

NTD, N-terminal domain; RBD, receptor binding domain; SD1 and SD2, subdomain 1 and 2; FP, fusion peptide; HR1 and HR2, heptad repeat 1 and 2; TM, transmembrane domain; CT, cytoplasmic tail. b, Schematic illustration of the production process of the SARS-CoV-2 vaccine using VLP platform. c, Electron microscopy image of VLP. Scale bar, 100 nm. d, Copy number of spike mRNA in each VLP particle. The copy number was detected by absolute quantification RT-qPCR and normalized to IDLV S-mut (2 copies RNA per virion). e, Western blot analysis of the spike protein in the virion treated with/without PNGase F. IDLV use as a control. 100 ng p24 for each vector. f, Western blot analysis of the spike protein expression. 293T cells were collected 36 h after transfection or transduction. 300 ng p24 virus or VLP used for each well. g. Confocal analysis of spike protein expression. 293T cells were fixed 36 h after transfection or transduction. Images are representative of three independent biological replicates in one experiment. h-j, Innate immune response induced by VLP in THP-1 derived macrophages. Cells were harvested for IFNB1, ISG15 and RIG-I analysis by RT-qPCR 6 h after transduction. 150 ng p24 per well for IDLV S-mut or VLP S-mut. 1.5 μg poly I:C per well as positive controls. ***P< 0.0001 (h-j). S represents spike. S-mut represents mutant spike. Data and error bars represent mean ± s.e.m.; one-way ANOVA with Dunnett’s post hoc tests were performed; n.s.=non-significant.

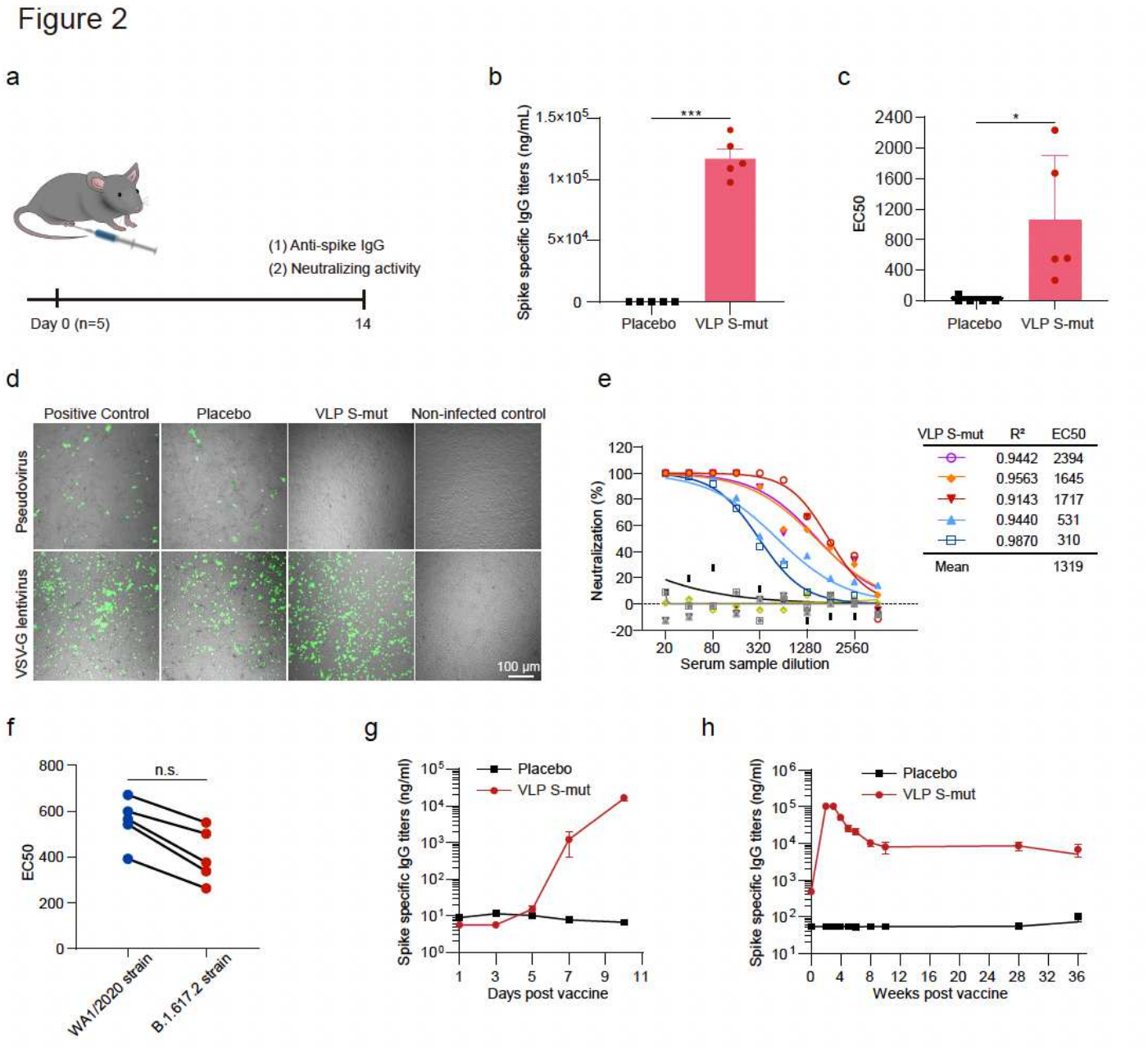

Figure 2

VLP mRNA induces robust and durable spike-specific antibody responses. a, Schematic illustration of the working plan (n=5). The sera were collected 14 days after footpad VLP injection for further analysis. b, ELISA analysis of spike specific IgG. ***P< 0.0001. c-f, Neutralization activity of vaccinated sera evaluated by luciferase assay (c and f), confocal microscopy (d) and plaque assay(e). A firefly luciferase-encoding pseudovirus, GFP-expressing SARS-CoV-2 pseudovirus and live SARS-CoV-2 (USA-WA1/2020) was used, respectively, to transduce Huh-7 or Vero E6 cells. *P= 0.0260 (c). Images are representative of three independent biological replicates in one experiment (d). g and h, Antibody changes in short-term (g) and long-term (h) follow-up vaccination. Mice were immunized with 1.5 μg VLP S-mut via footpad injection, sera were collected at the indicated time for IgG ELISA. Data and error bars represent mean ±

s.e.m.; unpaired two-tailed student's t-tests (b and c); two-tailed Wilcoxon matched-pairs 1 signed-rank test (f).

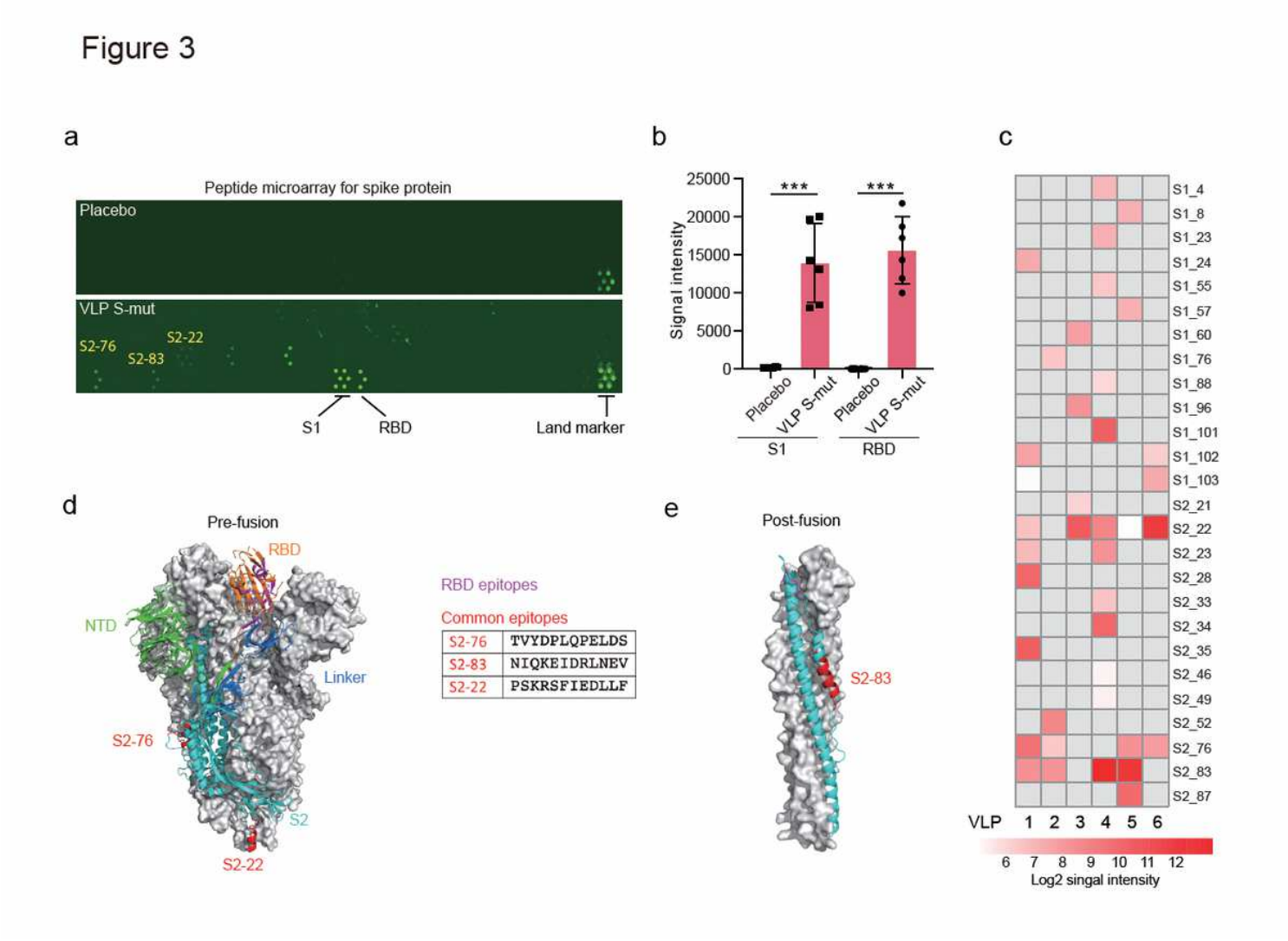

Figure 3

Linear epitope landscape in the VLP mRNA vaccinated mice. a, Representativ images of spike peptide microarray. S1 protein and RBD were included in the microarray as controls. Highly frequent positive peptides were labeled. b. Antibody responses against S1 protein or RBD in vaccinated mice. Signal intensity was averaged fluorescent intensity of tinplated spots for each array. ***P< 0.0001. c, Heatmap of antibody responses against peptides. The gray grid indicates a negative response. d and e, Analysing the epitopes of VLP induced spike-specific antibodies on spike protein. 6 mice were used for each group, 1.5 μg VLP S-mut or 50 μL PBS were injected via footpad into each mouse. Data and error bars represent mean ± s.e.m.; unpaired two-tailed student's t-tests.

Figure 4

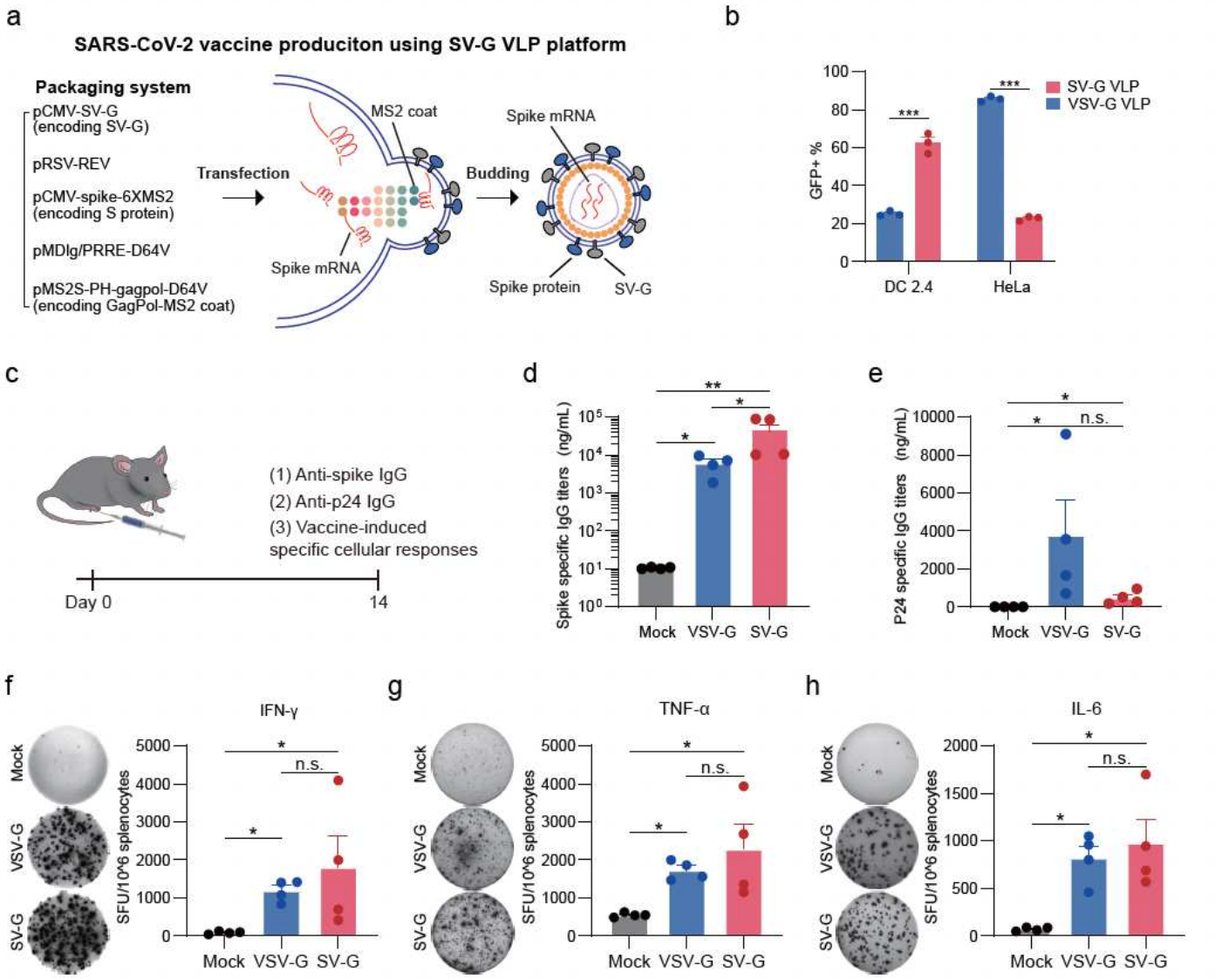

Figure 4

DC-targeting VLP-mRNA vaccine induced enhanced spike-specific IgG and T cell immune response. a, Illustration of the production process of the DC-specific VLP-mRNA vaccine. b, Evaluating the DC-specificity of SV-G pseudotyped VLP. 100 ng p24 GFP mRNA-carrying VLP pseudotyped by SV-G and VSV-G, respectively, were transduced to 4x104 DC 2.4 or HeLa cells. Three days later, the transduction efficiency was measured by flow cytometry analysing the GFP expression. ***P =0.0003 of DC2.4 and ***P< 0.0001 of Hela for SV-G VLP versus VSV-G VLP. c, The working plan for analysing VLP mRNA elicited the humoral and cellular immune responses. d and e, ELISA analysis of spike specific and p24 specific IgG. Serum was collected at 14 days post-immunization (1.5 μg p24 VLP per mouse, n=4 mice). *P = 0.0286 for all groups (d). *P = 0.0286 for Mock versus VSV-G and Mock versus SV-G, *P = 0.0571 for VSV-G versus SV-G (e). f-h, Quantification of the number of IFN-γ, TNF-α and IL-6 spot-forming cells

isolated from the spleen after stimulation with spike peptide pool. *P = 0.0286 for all groups (f-h). Representative images of ELISPOT wells showed on left. Images are representative of three independent biological replicates in one experiment. Data and error bars represent mean ± s.e.m.; unpaired two-tailed Mann-Whitney tests (d, e, f-h) ; n.s.=non-significant.

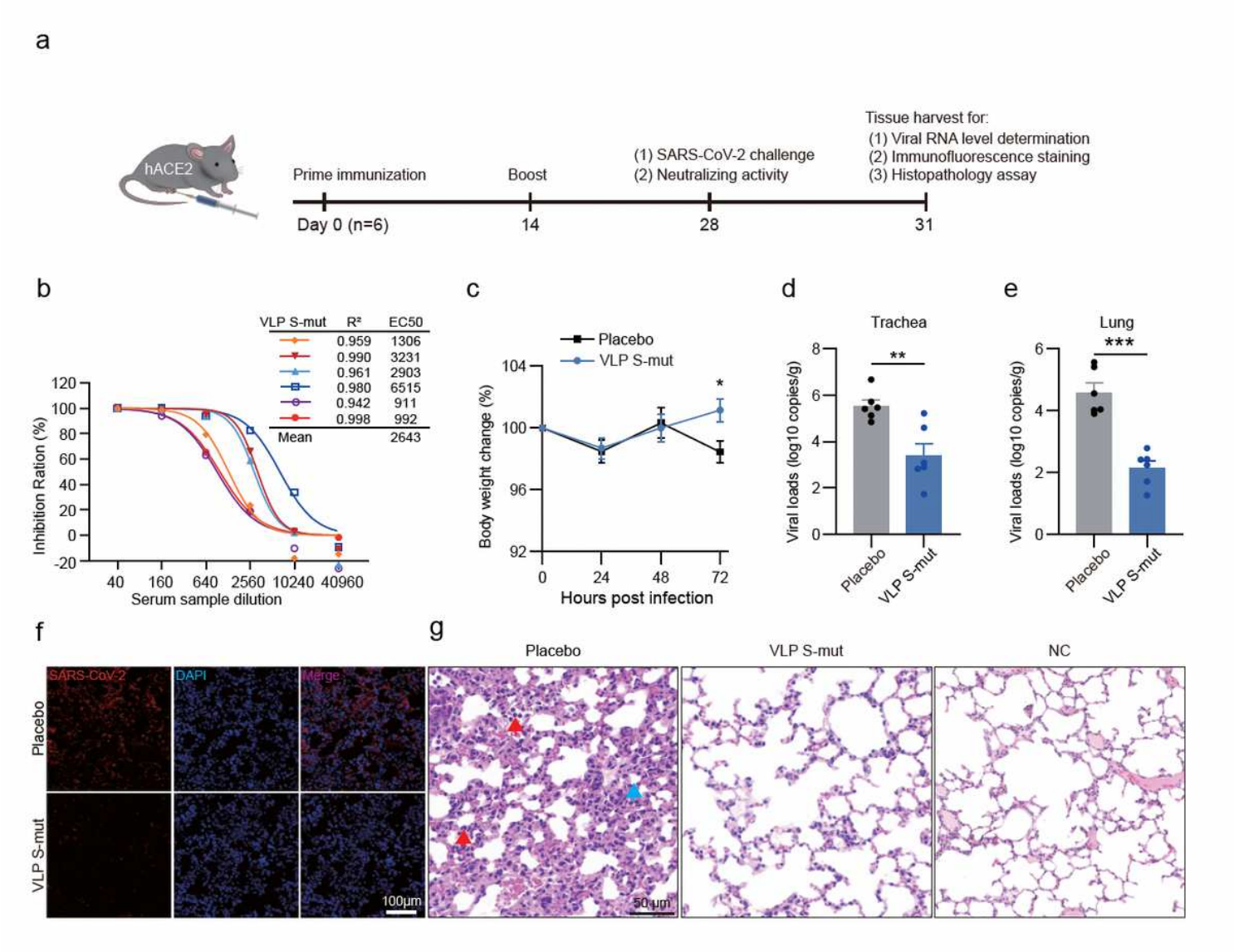

Figure 5

DC-specific VLP-mRNA vaccine efficiently protected hACE2 transgenic mice from the SARS-CoV-2 challenge. a, Scheme of vaccination and challenge. 1.5 μg p24 SV-G VLP or 50 μL PBS were immunized by footpad injection (n=6), and boosted at 14 days post prime immunization. Mice were challenged with 105 TCID50 of SARS-CoV-2 at 14 days post boos immunization by intranasal administration. All mice were euthanized at 3 d.p.i. b, Neutralizatio activity of vaccinated sera against live SARS-CoV-2 (USA-WA1/2020). c, The percentage of mic weight change after infection. *P = 0.0253. d and e, Viral loads in lung and trachea detected by RT-qPCR. f, Confocal analysis of SARS-CoV-2 in the lung. **P = 0.0042 (d) and ***P < 0.0001 (c). g, Lung histopathology analysis by hematoxylin and eosin (red arrow,

inflammatory cell infiltration; blue arrow, alveolar destruction). Each image is a representative of a group of 4 mice (f and g). Data and error bars represent mean ± s.e.m.; unpaired two-tailed student's t-tests (c-e).

Figure 6

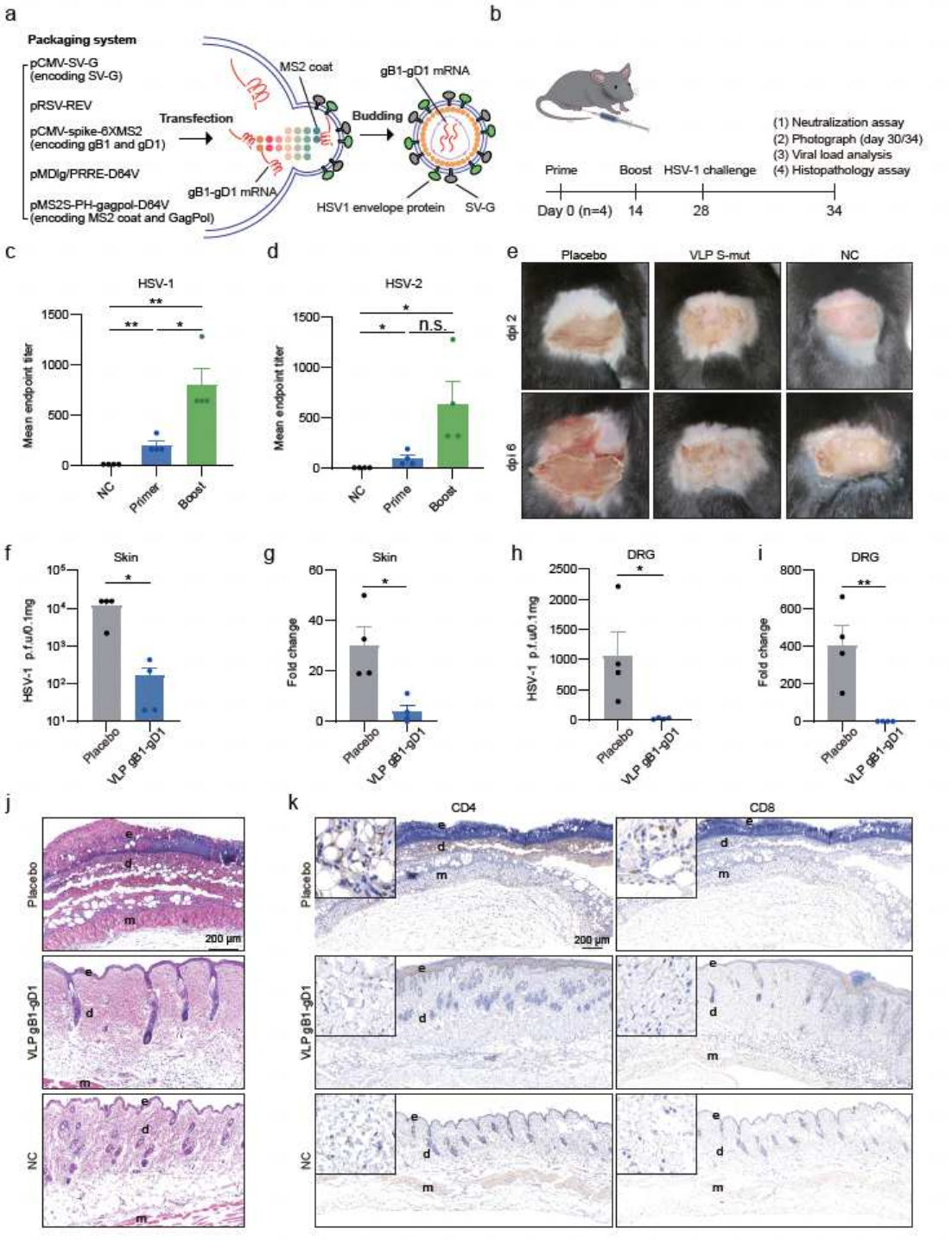

Figure 6

DC-specific VLP-mRNA co-delivering gB1 and gD1 efficiently protected mice from the HSV-1 infection. a, Schematic illustration of the production process of the VLP gB1-gD1 vaccine. b, Flowchart for analysing the effectiveness of VLP gB1-gD1 vaccination against HSV-1 infection. Six-week-old C57BL/6 mice (n=4)

were immunized with 2 μg p24 VLP mRNA vaccine at day 0 and day 14, respectively. c and d, Neutralization activity against live HSV-1 and HSV-2. n=4 mice. **P = 0.0032 for Prime versus NC, **P = 0.0026 for Boost versus NC and *P = 0.0109 for Prime versus Boost (c). *P = 0.0365 for Prime versus NC, *P = 0.0309 for Boost versus NC (d). e, Representative images of skin at 2 d.p.i. and 5 d.p.i. Each image is representative of four mice in one experiment. f and g, Plaque assay and qPCR analysis of the HSV-1 replication in the skin at 6 d.p.i. *P = 0.0113 (f), *P = 0.0147 (g). h and i, Plaque assay and qPCR analysis of the HSV-1 replication in the DRG at 6 d.p.i. *P = 0.0437 (h), **P = 0.0088 (i). j, HE analysis of skin histopathology at 6 d.p.i. k, IHC analysis of CD4+ and CD8+ T cells infiltration in the skin 6 days after infection. e, epidermis; d, dermis; m, muscle. Each image is a representative of four mice in one experiment (e, j and k). Data and error bars represent mean ± s.e.m.; unpaired two-tailed Student's t-tests (c, d, f- i); n.s.=non-significant.

Supplementary Files

This is a list of supplementary files associated with this preprint. Click to download.

- SupplementaryTablesYinetaltoNBT.docx
- SupplementaryFiguresYinetaltoNBT.docx